Fully integrated graphene electronic biosensor for label-free detection of lead (II) ion based on G-quadruplex structure-switching

Yijun Li, Cheng Wang, Yibo Zhu, Xiaohong Zhou, Yu Xiang, Miao He, Siyu Zeng

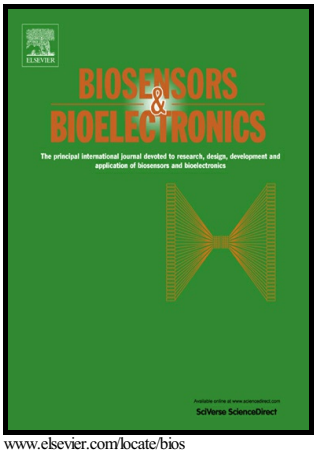

www.elsevier.com/locate/bios

PII: S0956-5663(16)31074-0
DOI: http://dx.doi.org/10.1016/j.bios.2016.10.061
Reference: BIOS9283

To appear in: *Biosensors and Bioelectronic*

Received date: 11 July 2016
Revised date: 17 October 2016
Accepted date: 20 October 2016

Cite this article as: Yijun Li, Cheng Wang, Yibo Zhu, Xiaohong Zhou, Yu Xiang, Miao He and Siyu Zeng, Fully integrated graphene electronic biosenso for label-free detection of lead (II) ion based on G-quadruplex structure s w i t c h i n g , *Biosensors and Bioelectronic* http://dx.doi.org/10.1016/j.bios.2016.10.061

Fully integrated graphene electronic biosensor for label-free detection of lead (II) ion based on G-quadruplex structure-switching

Yijun Li[a,b], *Cheng Wang*[a,b*], *Yibo Zhu*[c], *Xiaohong Zhou*[a,b], *Yu Xiang*[d], *Miao He*[a,b], *Siyu Zeng*[b*]

[a]Center for Sensor Technology of Environment and Health, Tsinghua University, Beijing 100084, China

[b]State Key Joint Laboratory of Environmental Simulation and Pollution Control, School of Environment, Tsinghua University, Beijing 100084, China

[c]Department of Mechanical Engineering, Columbia University, New York, NY 10027, USA

[d]Department of Chemistry, Tsinghua University, Beijing 100084, China

cwang@tsinghua.edu.cn

szeng@tsinghua.edu.cn

[*]Corresponding author.

Abstract

This work presents a fully integrated graphene field-effect transistor (GFET) biosensor for the label-free detection of lead ions (Pb^{2+}) in aqueous-media, which first implements the G-quadruplex structure-switching biosensing principle in graphene nanoelectronics. We experimentally illustrate the biomolecular interplay that G-rich DNA single-strands with one-end confined on graphene surface can specifically interact with Pb^{2+} ions and switch into G-quadruplex structures. Since the structure-switching of electrically charged DNA strands can disrupt the charge distribution in the vicinity of graphene surface, the carrier equilibrium in graphene sheet might be altered, and manifested by the conductivity variation of GFET. The measurements of Pb^{2+} samples and theoretical analysis show that our devices are capable of the label-free and specific quantification of Pb^{2+} with a detection limit down to 163.7 ng/L. These results first verify the signaling principle competency of G-quadruplex structure-switching in graphene electronic biosensors. Combining with the advantages of the compact device structure and convenient electrical signal, a label-free GFET biosensor for Pb^{2+} monitoring is enabled with promising application potential.

Graphical abstract

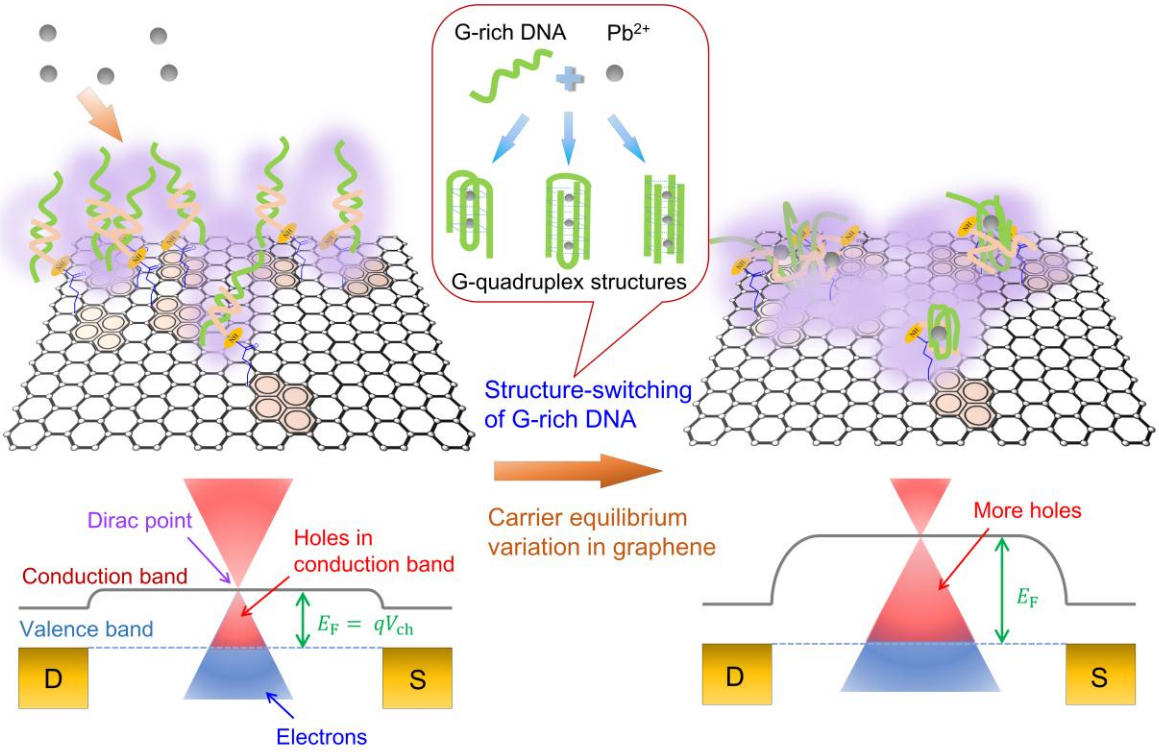

Keywords: graphene field-effect transistor, fully integrated biosensor, lead (II) ion, G-quadruplex, structure-switching signaling

1. Introduction

Lead ion (Pb^{2+}), a widespread heavy metal pollutant in the water environment(Guo et al. 2014), has become a severe threat to human health, due to its long-lasting, cumulative detrimental effects(Needleman 2004). To strengthen the control of Pb^{2+} pollutions, efficient and reliable detection techniques are of great significance. Nowadays, Pb^{2+} detections in aqueous-media commonly rely on instrumental methods, such as atomic absorption spectroscopy (AAS), atomic emission spectrometry (AES) and inductively coupled plasma mass spectrometry

(ICP-MS)(Duarte et al. 2016; Foltynová et al. 2014; Sixto et al. 2016). Although these techniques are capable of the accurate quantification of Pb^{2+}, the needs for expensive equipment and professional operations still hinder further applications. As a result, novel sensor techniques, as well as analytical tools, for rapid, simple and convenient Pb^{2+} detections, have been attracting more and more research interests.

Recently, biosensors exploiting specific biorecognition principles for Pb^{2+} detection have been reported. As the functional nucleic acid researches revealed(Beissenhirtz and Willner 2006; Liu et al. 2009), selected oligonucleotide sequences specifically responsive to Pb^{2+} (i.e., DNAzyme and G-quadruplex) can be employed as the pivot receptors(Han et al. 2016; Li et al. 2009). Herein, similar to the DNAzyme-based Pb^{2+} biosensors relying on the specific binding or cleavage of designated site(Wang et al. 2015b), the G-quadruplex-based methods can achieve the signaling of Pb^{2+} recognition via the DNA structure-switching(Kong et al. 2009; Neidle and Read 2000; Parkinson et al. 2002). Although the utility of G-quadruplex has been demonstrated in the development of Pb^{2+} biosensors, the signal readout still required laboratory analytical instruments, such as electrochemical and optical platforms(Guo et al. 2012; Li et al. 2010; Lin et al. 2011). To our knowledge, integrated G-quadruplex biosensor, which is freed from the instrument restriction and capable of the convenient Pb^{2+} detection in an on-line mode like the DNAzyme-based electronic Pb^{2+} biosensor(Wang et al. 2016a), is yet to be fulfilled.

Here, we present a novel biosensor that first incorporates the G-quadruplex structure-switching signaling principle in a graphene electronic nanodevice for the label-free

Pb^{2+} detection in aqueous-media. We consider that DNA molecules in aqueous-media are naturally charged with negative electricity (DNA isoelectric point is about pH 5)(Stotzky 2000), and the charge distribution is related to the DNA secondary structure. Thereby, the DNA structure-switching may enable a label-free sensing principle that transduces biomolecular interactions into electrical signals via the charge redistribution on semiconductors(Chen et al. 2008). To realize this principle, we choose graphene, the most sensitive electronic material people ever discovered(Novoselov et al. 2005), to fabricate sensor devices. As a two-dimensional semiconductor with extraordinarily high carrier mobility(Ponomarenko et al. 2009), the carrier equilibrium fluctuation in graphene reflecting interfacial biomolecular interactions can be observed through conductivity variations under the graphene field-effect transistor (GFET) configuration(Cai et al. 2015; Cai et al. 2014; Chen et al. 2013; Kwak et al. 2012; Ohno et al. 2010a, b; Saltzgaber et al. 2013; Wang et al. 2016a; Yan et al. 2014; Yin et al. 2011). In addition, to offer our devices a fully integrated structure for the convenient application, a high-κ solid-gate GFET configuration(Wang et al. 2016b; Zhu et al. 2015) is utilized in this work (Fig. 2). Compare to the conventional liquid-gate GFET biosensors, our devices eliminate the structural instability due to the external wire gate electrode(Wang et al. 2015a; Zhu et al. 2016), and thus fundamentally overcome the device reliability hindrance in practical applications.

The sensing principle is designed as shown in Fig. 1. While the graphene sheet is immerged in aqueous-solution (Fig. 1a), an electrical double layer (EDL) is formed on the hydrophobic

graphene surface(Bonthuis et al. 2011; Rafiee et al. 2012). Changes of electric properties arising from the interfacial biomolecular interactions can be designed to enable the Pb^{2+} detection(Hepel 2012; Hepel et al. 2012; Stobiecka et al. 2010; Stobiecka and Hepel 2011). From the viewpoint of GFET electronics, the one-end immobilized DNA strands carry negative charges by ionization in solution(Stotzky 2000), and electrostatically induce holes in graphene through the equivalent EDL capacitance. Hence, the graphene sheet may exhibit a positive chemical potential V_{ch} (Novoselov et al. 2005), which renders the GFET a *p*-type doping performance (see electrical modeling and energy band diagrams in Fig. 1a). Meanwhile, the Debye screening effect on DNA charges has to be taken into account. For instance, in physiological saline solutions (ionic strength I ~150 mM), the electrostatic potential of a point charge exponentially decreases with distance and approaches its $1/e$ at the Debye length $\lambda_{\mathrm{D}} \approx 0.7$ nm. Thereby, the charged nucleotides away from the charge plane of EDL farther than the induction range (~2 nm) may not effectively induce holes in graphene(Sorgenfrei et al. 2011). While the DNA strands interact with Pb^{2+} ions and fold into G-quadruplex structures (Fig. 1b)(Kong et al. 2009; Neidle and Read 2000; Parkinson et al. 2002), more charged nucleotides might be brought into the induction range that increase the hole density in graphene(Wang et al. 2016b). As a result, the GFET may exhibit an increasing *p*-doping effect and corresponding conductivity responses that enable the label-free biosensing of Pb^{2+} (Fig. 1c). In addition, we note that the G-quadruplex formation may also incorporate Pb^{2+} ions into the induction range, which is prone to neutralize a part of the negative charges. Here, on the basis of previous investigations(Kong et al. 2009; Neidle and Read 2000; Parkinson et al. 2002), we conjecture that the hole density increase in graphene led by

G-quadruplex structure-switching plays the dominant role.

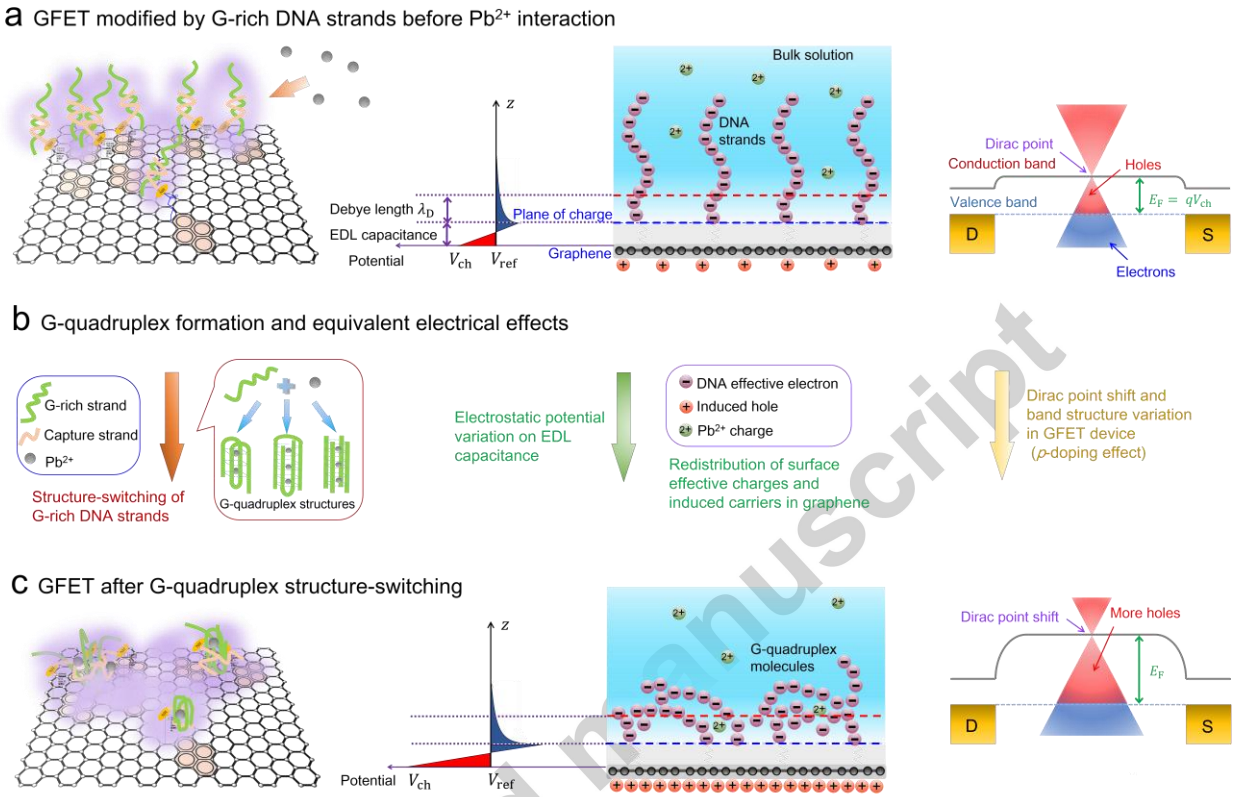

Fig. 1. G-quadruplex structure-switching principle and schematic illustrations of electrical response mechanism on GFET. (a) Before G-quadruplex formation: Along *z* axis (upward direction perpendicular to graphene surface), charges distributing on the distal ends of DNA strands cannot effectively apply electrostatic potential onto the charge plane of EDL capacitance due to the Debye screening. The effective hole density and chemical potential (V_{ch}) of graphene are relatively low. The GFET exhibits a slight *p*-type doping performance. (b) In the presence of Pb^{2+}: G-rich DNA strands switch into the G-quadruplex structures, and thus lead to changes of electric properties. (c) After G-quadruplex structure-switching: More DNA charges move closer to the charge plane of EDL that increase the hole density in graphene, and thus strengthens the *p*-type doping of GFET.

2. Materials and methods

2.1. Chemicals and materials

Copper foil (99.8%, 25 μm thick) for the chemical vapor deposition (CVD) graphene synthesis was purchased from Alfa Aesar (Ward Hill, MA). Silicon wafers (*n*-type, 1 μm SiO_2-coated) for device substrate were purchased from Crystal-Silicon Electronics (Suzhou, China). Polydimethylsiloxane (PDMS) for microfluidics was purchased from Dow Corning (Midland, MI). 1-pyrenebutanoic acid succinimidyl ester (PASE), 4-(2-hydroxyethyl)-1-piperazineethanesulfonic acid (HEPES) were purchased from Sigma-Aldrich (St. Louis, MO). Standard solutions of heavy metal ions were obtained from National Center of Analysis and Testing for Nonferrous Metals and Electronic Materials (Beijing, China). G-rich DNA strand (5′–GGG TGG GTG GGT GGG T–3′) and amino-modified DNA capture strand (5′–CAC CCT CCC AC-NH_2–3′) were customized from Sangong Biotech. (Shanghai, China).

2.2. Device

The sensor devices were designed on the basis of a high-κ solid-gate GFET configuration (Fig. 2a), and fabricated using wafer-scale MEMS techniques for mass production (Fig. 2b). Detailed fabrication protocol are provide in Supplementary information (Fig. S1 and S2). Briefly, a planar metal gate electrode is first patterned on the SiO_2/Si substrate and buried by a 30 nm HfO_2 dielectric layer to replace the wire electrode in liquid-gate GFET nanosensors. After the

patterning of drain/source electrodes, a monolayer CVD graphene sheet is transferred to create the conducting channel (see Fig. S1 for the graphene transfer technique and quality characterization details). As the scanning electron microscopy image shown in Fig. 2b, the graphene conducting channel is accurately gated by the planar gate electrode. To handle sample solutions in subsequent experiments, the GFET device is packaged by an elastic PDMS microfluidic channel (Fig. 2b).

The test circuitry (Fig. 2a) uses a triple DC power supply (E3631A, Keysight) to provide a drain voltage (V_{ds}), and a waveform generator (33500B, Keysight) to supply an adjustable gate voltage (V_{gs}). A digital multimeter (33410A, Keysight) is connected in the drain-source loop to measure the drain current (I_{ds}). The measurement is controlled through a Labview program.

To realize our sensing principle (Fig. 1), the graphene conducting channel is biochemically functionalized (see detailed protocol and characterization results in Fig. S3)(Wang et al. 2015a). First, the PASE linker molecules are absorbed onto graphene surface via the irreversible π-π stacking. Then the DNA capture strands are immobilized through the amino-group condensation. And the G-rich DNA strands are captured on graphene surface to complete the functionalization.

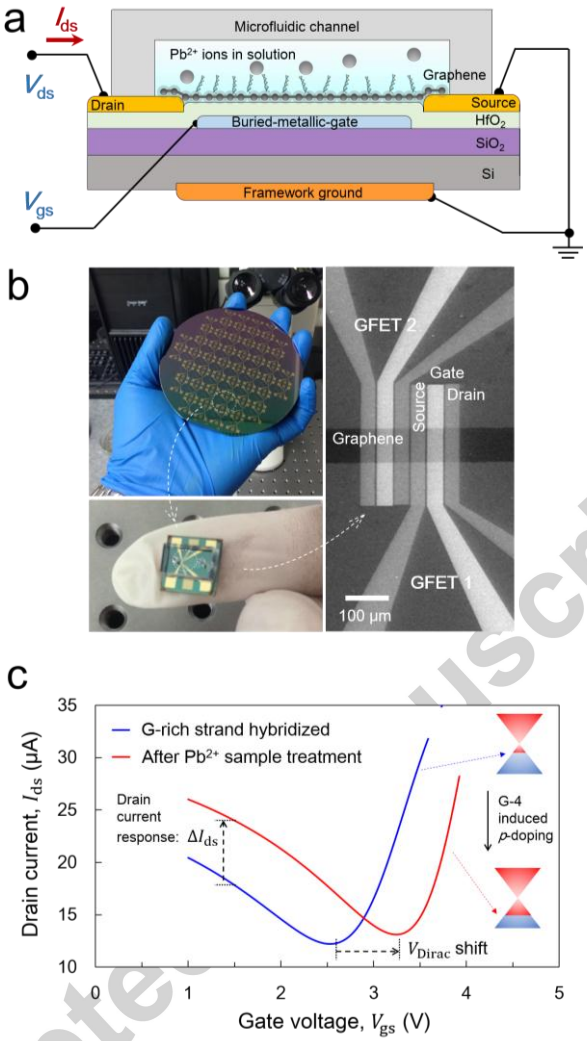

Fig. 2. Schematic, fabrication and electrical characterization of sensor device. (a) Device schematic and electrical connection of the test circuitry. (b) Wafer-scaled fabrication of GFET devices. Each single device was packaged by a PDMS microfluidic channel for the liquid handling. The GFET unit in a device was observed through scanning electron microscopy. (c) Transfer characteristics of a biochemically functionalized GFET device at room temperature (Buffer solution: 1x HEPES buffer (pH 7.2, I ~150 mM); Drain bias voltage: V_{ds} = 30 mV).

3. Results and discussion

3.1. Electrical characterization

To verify the validity of the sensing principle in Fig. 1, a functionalized GFET device was electrically characterized in 1x HEPES buffer (pH 7.2, containing HEPES and $NaNO_3$ 50mM, respectively) at room temperature. As displayed in Fig. 2c, two ambipolar curves measured under the drain voltage V_{ds} = 30 mV show the GFET transport characteristic variation before and after the treatment of a concentrated Pb^{2+} sample (500 μg/L). The positive shift of the charge neutrality point (denoted V_{Dirac}) suggests a *p*-type doping effect, which is in agreement with the sensing principle we proposed in Fig. 1 that G-rich DNA strands switch into G-quadruplex structures. Besides, we also found that the transfer characteristic variation (Fig. 2c) allows us to study the Pb^{2+}-induced interactions via the continuous measurements of drain current I_{ds} at a fixed gate voltage V_{gs}.

3.2. Analyte detections

The Pb^{2+} detection experiments were then carried out at room temperature. The Pb^{2+} samples at various concentrations (0 to 500 μg/L) were prepared using 1x HEPES buffer (pH 7.2, I ~150 mM). To achieve a wide dynamic range of I_{ds} variations reflecting the Pb^{2+}-induced interactions, the gate voltage was set to V_{gs} = 1.5 V in this work (see electrical characterization results in Fig. 2c). In addition, to prevent the device damage risk in aqueous-media, which is potentially caused by the electrochemical erosion of the electrode adhesive metal layer (Wang et

al. 2015a), the drain voltage in subsequent tests was limited to V_{ds} = 30 mV to guarantee I_{ds} always lower than 30 μA, at V_{gs} = 1.5 V. While a sample was introduced into microfluidic channel, $I_{ds}(t)$ was recorded over time to depict the biosensing interaction process.

As shown in Fig. 3a – 3h, the Pb^{2+} detection results observed from a device indicate that a time-resolved response (denoted $\Delta I_{ds}(t)$) exponentially increases and eventually arrives to the equilibrium (denoted ΔI_{ds}^{eq}). And the ΔI_{ds}^{eq} level is positively related to the Pb^{2+} concentration c. This phenomenon suggests that a higher Pb^{2+} concentration may motivate more G-rich DNA strands transforming into G-quadruplex structures. Furthermore, we also discovered a concentration-dependent saturation behavior of ΔI_{ds}^{eq} in Fig. 3g and 3h, which might be understood as the complete G-quadruplex formation of G-rich strands while Pb^{2+} sample is sufficiently concentrated. Hence, we define the equilibrium response $\Delta I_{ds}^{eq}(c)$ at c = 500 μg/L as the saturated response ΔI_{ds}^{sat} for each device, and normalize the concentration-dependent equilibrium responses as the Pb^{2+}-induced G-quadruplex formation ratio, $R(c) = \Delta I_{ds}^{eq}(c)/\Delta I_{ds}^{sat}$, to eliminate the errors caused by device-to-device nonuniformity.

By plotting the normalized equilibrium responses against Pb^{2+} concentration as shown in Fig. 3i, we found a Hill-Langmuir relationship(Lerner et al. 2013) that accurately describes the G-quadruplex formation manner with respect to the stoichiometry of Pb^{2+}:

$$R(c) = A\frac{c^n}{c^n + {K_{1/2}}^n} + (1 - A) \qquad (1)$$

By fitting Eq. (1) to the experimental data, three parameters A, n and $K_{1/2}$ were determined. Here, A = 0.773 defines the dynamic range of the normalized sensor response arising from G-quadruplex formation. The Hill coefficient, n = 0.602, suggests that the Pb^{2+}-induced G-quadruplex formation involves cooperative interactions(Gesztelyi et al. 2012) among adjacent G-rich strands. This suggestion is in coincidence with previous bimolecular interplay investigations(Kong et al. 2009; Neidle and Read 2000; Parkinson et al. 2002), and our sensing principle design in Fig. 1. In particular, the effective affinity constant $K_{1/2}$ = 5.814 μg/L indicates a Pb^{2+} concentration scale in the G-quadruplex formation(Weiss 1997). At $c = K_{1/2}$, the sensor response reaches half of the dynamic range: $R(K_{1/2}) = R(0) + A/2$ (see inset of Fig. 3i). Hence, smaller $K_{1/2}$ value renders sensor devices better capability in the quantification of low concentration Pb^{2+} ions. Under the normal noise conditions, the detectable concentration would be no higher than the $K_{1/2}$ level.

3.3. Sensing performance

We then estimate the limit of detection (LOD) performance of our sensor devices in the quantification of Pb^{2+} concentration. First, on the basis of experimental data, the standard deviation level of the sensor responses is statistically determined as σ_R = 0.0269. Then, a specific Pb^{2+} concentration which yields the sensor response a confidential variation, three times the σ_R value, is defined as the LOD following the $''3\sigma''$ rule(Homola 2008). As the calibration curve Eq. (1) is non-linear, the LOD concentration of $Pb^{2+}$is calculated via its inverse function:

$$c(R) = K_{1/2}\sqrt[n]{\frac{R + A - 1}{1 - R}}$$

While $R(0) = 1 - A$, we get LOD = $c(1 - A + 3\sigma_R)$ = 163.7 ng/L (see Supplementary information Fig. S4 for calculation details (Biagini et al. 2004; Holstein et al. 2015; Ingle Jr and Wilson 1976; Tschmelak et al. 2006)). This level, achieved by a label-free biosensing method, is well below the performance requirements of drinking water Pb^{2+} monitoring (allowable concentration ~50 μg/L), and blood lead test (safe level ~100 μg/L).

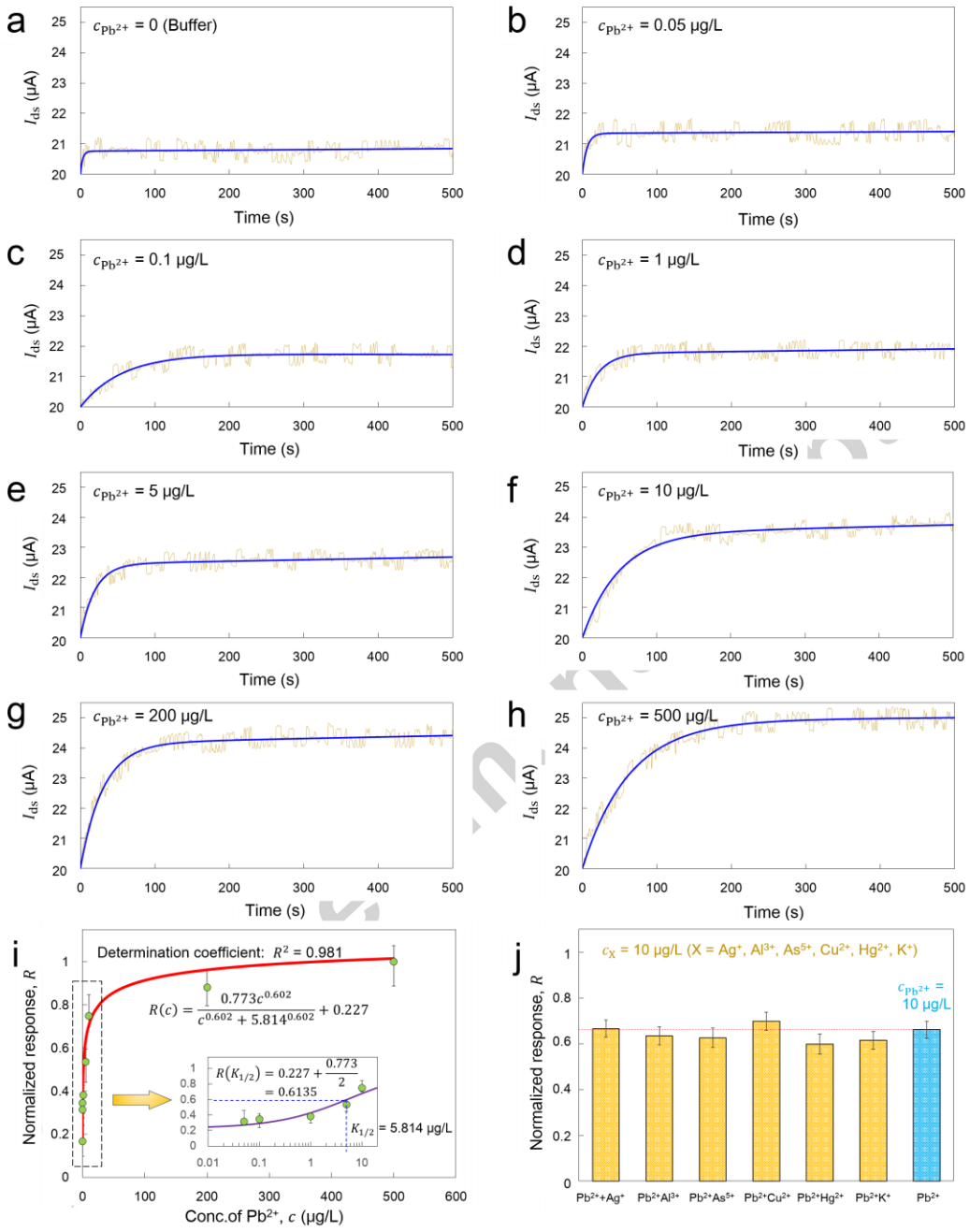

Fig. 3. Measurement results of the Pb^{2+} sensing experiments. Kinetic response measurements of Pb^{2+} samples (prepared using 1x HEPES buffer, pH 7.2, I ~150 mM) at (a) c = 0 μg/L, (b) c = 0.05 μg/L, (c) c = 0.1 μg/L, (d) c = 1 μg/L, (e) c = 5 μg/L, (f) c = 10 μg/L, (g) c = 200 μg/L, and (h) c = 500 μg/L. All the measurements were conducted at room temperature, under the electrical conditions V_{gs} = 1.5 V and V_{ds} = 30 mV. In (a) – (h), experimental data are fitted by exponential functions (blue solid curves). (i) Normalized

equilibrium responses at various Pb^{2+} concentrations (Error bars represent the maximum and minimum values from multiple measurements at each concentration). The concentration-dependent relationship is fitted by a Hill-Langmuir equation (red solid curve, determination coefficient R^2 = 0.981). (j) Results of control experiments. Control samples containing 10 μg/L Pb^{2+} and 10 μg/L disruptor ion (Ag^+, Al^{3+}, As^{5+}, Cu^{2+}, Hg^{2+} and K^+, respectively) were tested under the same experimental conductions.

Moreover, to verify the biosensing specificity of Pb^{2+} ions, control experiments detecting samples mixed by disruptors were conducted. As shown in Fig. 3j, metal ion disruptors (10 μg/L Ag^+, Al^{3+}, As^{5+}, Cu^{2+}, Hg^{2+} and K^+, respectively) do not significantly deviate the responses. And the Pb^{2+} detections executed in real water samples (drinking water and tap water samples) also exhibit reliable results (Supplementary information Fig. S5). These results suggest that our graphene biosensor designed based on the G-quadruplex structure-switching principle is specific to Pb^{2+} ions.

4. Conclusion

In this work, the utility of the G-quadruplex structure-switching signaling principle was demonstrated for the first time in the electronic biosensing of Pb^{2+} ions. By conducting the Pb^{2+} detections on a fully integrated GFET nanosensor, we experimentally suggested that G-rich DNA strands on the solution-solid interface (i.e., graphene surface) can switch into G-quadruplex structures in the presence of Pb^{2+} ions. As a result, a label-free Pb^{2+} sensing principle is enabled that the G-quadruplex formation induced DNA structure-switching can significantly alter the charge distribution on graphene surface, and thus excite GFET conductivity responses. As the experimental results showed that our GFET devices can quantify Pb^{2+} concentration with a LOD

level down to 163.7 ng/L, we confirm that the G-quadruplex structure-switching GFET biosensor holds great potential for the label-free monitoring of Pb^{2+} ions, and might be applicable in the detection of other appropriate targets.

Acknowledgements

This work was supported by the National High-Tech R&D (863) Program of China (2014AA06A506), the Major Scientific Equipment Development Project of China (2012YQ030111), the National Natural Science Foundation of China (21377065), the China Postdoctoral Science Foundation (2016M590104), and the Natural Science Foundation of Beijing (2162017). Y.L. and C.W. acknowledge the Nanofabrication Technology Center at Tsinghua University for the technical assistance in device fabrication. Y.Z. acknowledges the National Scholarship (201206250034) from the China Scholarship Council.

Appendix A. Supplementary information

Supplementary information associated with this article is separately uploaded.

References

Beissenhirtz, M.K., Willner, I., 2006. Org. Biomol. Chem. 4(18), 3392-3401.

Biagini, R.E., Sammons, D.L., Smith, J.P., MacKenzie, B.A., Striley, C.A., Semenova, V., Steward-Clark, E., Stamey, K., Freeman, A.E., Quinn, C.P., 2004. Clin. Diagn. Lab. Immunol. 11(1), 50-55.

Bonthuis, D.J., Gekle, S., Netz, R.R., 2011. Phys. Rev. Lett. 107(16), 166102.

Cai, B., Huang, L., Zhang, H., Sun, Z., Zhang, Z., Zhang, G.-J., 2015. Biosens. Bioelectron. 74, 329-334.

Cai, B., Wang, S., Huang, L., Ning, Y., Zhang, Z., Zhang, G.-J., 2014. ACS Nano 8(3), 2632-2638.

Chen, J.-H., Jang, C., Adam, S., Fuhrer, M., Williams, E., Ishigami, M., 2008. Nat. Phys. 4(5), 377-381.

Chen, T.-Y., Loan, P.T.K., Hsu, C.-L., Lee, Y.-H., Tse-Wei Wang, J., Wei, K.-H., Lin, C.-T., Li, L.-J., 2013. Biosens. Bioelectron. 41, 103-109.

Duarte, Á.T., Borges, A.R., Zmozinski, A.V., Dessuy, M.B., Welz, B., de Andrade, J.B., Vale, M.G.R., 2016. Talanta 146, 166-174.

Foltynová, P., Bednařík, A., Kanický, V., Preisler, J., 2014. J. Anal. Atom. Spectrom. 29(9), 1585-1590.

Gesztelyi, R., Zsuga, J., Kemeny-Beke, A., Varga, B., Juhasz, B., Tosaki, A., 2012. Arch. Hist. Exact Sci. 66(4), 427-438.

Guo, D., Robinson, C., Herrera, J.E., 2014. Environ. Sci. Technol. 48(21), 12525-12532.

Guo, L., Nie, D., Qiu, C., Zheng, Q., Wu, H., Ye, P., Hao, Y., Fu, F., Chen, G., 2012. Biosens. Bioelectron. 35(1), 123-127.

Han, S., Zhou, X., Tang, Y., He, M., Zhang, X., Shi, H., Xiang, Y., 2016. Biosens. Bioelectron. 80, 265-272.

Hepel, M., 2012. Functional gold nanoparticles for biointerfaces. In: Hepel, M., Zhong, C.-J. (Eds.), Functional Nanoparticles for Bioanalysis, Nanomedicine, and Bioelectronic Devices, pp. 147-176. Oxford Univ. Press, Oxford.

Hepel, M., Blake, D., McCabe, M., Stobiecka, M., Coopersmith, K., 2012. Assembly of gold nanoparticles induced by metal ions. In: Hepel, M., Zhong, C.-J. (Eds.), Functional Nanoparticles for Bioanalysis, Nanomedicine, and Bioelectronic Devices, pp. 207-240. Oxford Univ. Press, Oxford.

Holstein, C.A., Griffin, M., Hong, J., Sampson, P.D., 2015. Anal. Chem. 87(19), 9795-9801.

Homola, J., 2008. Chem. Rev. 108(2), 462-493.

Ingle Jr, J., Wilson, R., 1976. Anal. Chem. 48(11), 1641-1642.

Kong, D.-M., Wu, J., Wang, N., Yang, W., Shen, H.-X., 2009. Talanta 80(2), 459-465.

Kwak, Y.H., Choi, D.S., Kim, Y.N., Kim, H., Yoon, D.H., Ahn, S.-S., Yang, J.-W., Yang, W.S., Seo, S., 2012. Biosens. Bioelectron. 37(1), 82-87.

Lerner, M.B., Dailey, J., Goldsmith, B.R., Brisson, D., Johnson, A.C., 2013. Biosens. Bioelectron. 45, 163-167.

Li, T., Dong, S., Wang, E., 2010. J. Am. Chem. Soc. 132(38), 13156-13157.

Li, T., Wang, E., Dong, S., 2009. J. Am. Chem. Soc. 131(42), 15082-15083.

Lin, Z., Chen, Y., Li, X., Fang, W., 2011. Analyst 136(11), 2367-2372.

Liu, J., Cao, Z., Lu, Y., 2009. Chem. Rev. 109(5), 1948-1998.

Needleman, H., 2004. Annu. Rev. Med. 55, 209-222.

Neidle, S., Read, M.A., 2000. Biopolymers 56(3), 195-208.

Novoselov, K.S., Geim, A.K., Morozov, S.V., Jiang, D., Katsnelson, M.I., Grigorieva, I.V., Dubonos, S.V., Firsov, A.A., 2005. Nature 438(7065), 197-200.

Ohno, Y., Maehashi, K., Matsumoto, K., 2010a. Biosens. Bioelectron. 26(4), 1727-1730.

Ohno, Y., Maehashi, K., Matsumoto, K., 2010b. J. Am. Chem. Soc. 132(51), 18012-18013.

Parkinson, G.N., Lee, M.P., Neidle, S., 2002. Nature 417(6891), 876-880.

Ponomarenko, L., Yang, R., Mohiuddin, T., Katsnelson, M., Novoselov, K., Morozov, S., Zhukov, A., Schedin, F., Hill, E., Geim, A., 2009. Phys. Rev. Lett. 102(20), 206603.

Rafiee, J., Mi, X., Gullapalli, H., Thomas, A.V., Yavari, F., Shi, Y., Ajayan, P.M., Koratkar, N.A., 2012. Nat. Mater. 11(3), 217-222.

Saltzgaber, G., Wojcik, P., Sharf, T., Leyden, M.R., Wardini, J.L., Heist, C.A., Adenuga, A.A., Remcho, V.T., Minot, E.D., 2013. Nanotechnology 24(35), 355502.

Sixto, A., Fiedoruk-Pogrebniak, M., Rosende, M., Cocovi-Solberg, D., Knochen, M., Miró, M., 2016. J. Anal. Atom. Spectrom. 31(2), 473-481.

Sorgenfrei, S., Chiu, C.-Y., Johnston, M., Nuckolls, C., Shepard, K.L., 2011. Nano Lett. 11(9), 3739-3743.

Stobiecka, M., Deeb, J., Hepel, M., 2010. Biophys. Chem. 146(2), 98-107.

Stobiecka, M., Hepel, M., 2011. Biosens. Bioelectron. 26(8), 3524-3530.

Stotzky, G., 2000. J. Environ. Qual. 29(3), 691-705.

Tschmelak, J., Kumpf, M., Käppel, N., Proll, G., Gauglitz, G., 2006. Talanta 69(2), 343-350.

Wang, C., Cui, X., Li, Y., Li, H., Huang, L., Bi, J., Luo, J., Ma, L.Q., Zhou, W., Cao, Y., 2016a. Sci. Rep. 6.

Wang, C., Kim, J., Zhu, Y., Yang, J., Lee, G.-H., Lee, S., Yu, J., Pei, R., Liu, G., Nuckolls, C., Hone, J., Lin, Q., 2015a. Biosens. Bioelectron. 71, 222-229.

Wang, C., Li, Y., Zhu, Y., Zhou, X., Lin, Q., He, M., 2016b. Adv. Funct. Mater. DOI: 10.1002/adfm.201602960.

Wang, R., Zhou, X., Shi, H., 2015b. Biosens. Bioelectron. 74, 78-84.

Weiss, J.N., 1997. FASEB J. 11(11), 835-841.

Yan, F., Zhang, M., Li, J., 2014. Adv. Healthcare Mater. 3(3), 313-331.

Yin, Z., He, Q., Huang, X., Zhang, J., Wu, S., Chen, P., Lu, G., Zhang, Q., Yan, Q., Zhang, H., 2011. Nanoscale 4(1), 293-297.

Zhu, Y., Hao, Y., Adogla, E.A., Yan, J., Li, D., Xu, K., Wang, Q., Hone, J., Lin, Q., 2016. Nanoscale 8(11), 5815-5819.

Zhu, Y., Wang, C., Petrone, N., Yu, J., Nuckolls, C., Hone, J., Lin, Q., 2015. Appl. Phys. Lett. 106(12), 123503.

Highlights

- The first demonstration of the DNA G-quadruplex structure-switching applied as a label-free electronic sensing principle.
- A newly-structured, fully-integrated graphene field-effect transistor (GFET) biosensor for Pb^{2+} detection in aqueous-media.
- An ideal limit of detection (LOD) level of Pb^{2+} concentration at ~163.7 ng/L.